Hindawi
Advances in Meteorology
Volume 2019, Article ID 4960624, 13 pages
https://doi.org/10.1155/2019/4960624

Research Article

Effects of Summer Rainfall on the Soil Thermal Properties and Surface Energy Balances in the Badain Jaran Desert

Jiangang Li,[1,2] **Ali Mamtimin**,[1,2] **Zhaoguo Li**,[3] **Cailian Jiang**,[4] **and Minzhong Wang**[1,2]

[1]*Institute of Desert and Meteorology, CMA, Urumqi 830002, China*
[2]*Center of Central Asian Atmospheric Science Research, Urumqi 830002, China*
[3]*Key Laboratory of Land Surface Process and Climate Change in Cold and Arid Regions, Northwest Institute of Eco-Environment and Resources, Chinese Academy of Sciences, Lanzhou 730000, China*
[4]*Wujiaqu Meteorology Bureau, Wujiaqu 831300, China*

Correspondence should be addressed to Ali Mamtimin; ali@idm.cn

Received 20 April 2019; Revised 11 October 2019; Accepted 13 November 2019; Published 6 December 2019

Academic Editor: Stefano Dietrich

Based on observational data collected during the summer of 2009 from the southern Badain Jaran Desert, the surface sensible and latent heat fluxes and shallow soil thermal storage were obtained through corrections and quality control measures. The soil thermal properties and characteristics of the land surface energy budget before and after rainfall episodes were systematically analyzed. Short-term precipitation had a greater influence than systematic precipitation on the soil temperature (ST) and soil volumetric water content (VWC). After rainfall, the VWC rapidly increased, showing a decreasing growth rate trend with depth and time in all layers; the soil temperature change rate (TCR) exhibited the opposite tendency. The surface albedo, which was affected little by the solar elevation angle and short-term precipitation, fluctuated from low to high during short-term rainfall. The soil thermal parameters, including the volumetric heat capacity, thermal conductivity, and diffusivity, all increased after rainfall. The diurnal soil heat flux variations in each layer manifested as quasisinusoids, and the amplitude gradually decreased with depth. The energy balance ratio (EBR) without and with soil heat storage (S) varied differently; after incorporating S, the EBR increased by approximately 5-6% regardless of rainfall but remained lower afterward. Throughout the observation period, the maximum daytime EBR appeared approximately 1-2 days before or after rainfall and gradually declined otherwise. These findings are fundamental for understanding the influences of cloud and precipitation disturbances on radiation budgets and energy distributions and improving the parameterization of surface radiation budgets and energy balances for numerical models of semiarid areas.

1. Introduction

Global warming not only leads to an increase in air temperature but also changes the amount, intensity, and frequency of precipitation [1]. Since the 20th century, the precipitation falling over the mid-high latitudes of the Northern Hemisphere has increased by approximately 7–12%, but the spatial distribution of this precipitation is uneven and exhibits a high degree of heterogeneity, which results in both an increased degree of uncertainty regarding the occurrence and duration of extreme precipitation and an enlargement of drought areas. The latter phenomenon intensifies hydrologic processes in terrestrial ecosystems, particularly in arid and semiarid areas [2, 3].

While partitioning of land surface fluxes, the soil has a larger role to play on the hydrological cycle as they are tightly connected with both land-atmosphere energy and water exchanges [4, 5]. Previous studies have shown that soil has a profound impact on the atmospheric surface layer, and the distribution and characteristic parameters of soil have certain effects on land-atmosphere energy exchange, water exchange, and the hydrological cycle [6–8]. The transport of both soil heat and water from the land surface to deeper layers is closely related to soil structure parameters, such as the soil composition, volume-weight ratio, humidity, and soil thermal parameters, including the soil thermal conductivity, thermal capacity, thermal diffusivity, and specific heat [9]. Accordingly, some researchers have studied the

thermal properties and heat fluxes of soil using a variety of methods and products [10–15], including the NOAH Land Surface Model (LSM) for estimating net radiation and latent, sensible, and ground heat (GH) fluxes as well as water balance components in four land treatments [16], a hydrological model for the simulation of soil moisture across multiple depths [17].

The majority of arid regions in Northwest China are desert or Gobi and are subject to intense solar radiation; as a result, the soil parameters are vastly different from those of typical regions, and the land surface physical processes therein exhibit notable regional characteristics [18]. Since the late 1980s, comprehensive field experiments have been carried out on land surface processes. The Heihe River field experiment (HEIFE) and the field experiment on the air-land interaction in the arid area of Northwest China (NWC-ALIEX) have confirmed certain soil parameters in the soil surface of their research regions [19–22]. However, comparatively speaking, specific research on the soil parameters in arid regions is still limited.

As the main water source in desert areas, precipitation has a considerable impact on the movement of dunes and the distribution of vegetation [23–27]. Due to limitations posed by the natural environment, only a small number of observation stations with an uneven spatial distribution are situated in the arid desert area of Northwest China; as a result, the characteristics of the soil physical parameters therein, specifically in the untraversed desert hinterlands, are poorly understood. Nevertheless, local meteorologists have conducted a large amount of research in the Taklamakan and Gurbantunggut Deserts, and their work has resulted in numerous achievements with regard to the effects of precipitation on deserts and their surrounding areas [28–30].

The Badain Jaran Desert is host to a variety of wavy landforms and sand mountains, the latter of which are the highest in the world, and these landforms have profound effects on rainfall. Zhang et al. analyzed the rainfall distribution in this region based on data from meteorological stations located around the desert [31]. However, few studies have investigated the effects of rainfall on the thermal properties of soil in deserts.

In this paper, hourly rainfall data acquired during the intense observation period (IOP, hereinafter) in the Badain Jaran Desert hinterland were integrated. Basic data, including the surface sensible heat flux, latent heat flux, and shallow soil thermal storage data, were obtained, and the surface albedo, soil volumetric heat capacity, thermal conductivity, thermal diffusivity, and energy balance ratio (EBR) were calculated by relevant equations. The effects of different types of rainfall on these soil characteristics and on the surface energy balances were analyzed, the results of which reveal the energy and water distributions in the underlying surface layer throughout the arid region of Northwest China.

2. Materials and Methods

2.1. Materials. The Badain Jaran Desert, located in the Alxa Banner of Inner Mongolia at approximately 39.5°–42°N and 98.5°–104°E, is the second-largest desert in China with an area of approximately 52,000 square kilometers [32]. This desert is mainly influenced by westerlies, namely, the Indian and East Asian monsoons, and belongs to temperate arid and extremely arid climate zones. The average annual precipitation exhibits a decreasing trend from the southeast (approximately 120 mm) to the northwest (less than 40 mm) [33]; precipitation primarily occurs from July to August. The northwest arid area, which is subject to a large amount of evaporation and abundant sunshine, is sensitive to climate change and possesses a fragile ecological environment. Hence, the northwest arid area is considered an ideal site to observe the water and heat exchanges in the underlying desert surface.

From June to September of 2009, researchers carried out a series of field observation experiments in the hinterland of the Badain Jaran Desert. The observation points were located in the southeast of the desert (39°28.122′N and 102°22.365′E at an altitude of 1418 m). The D1 observation site, which was surrounded by an open, undulating yellow sand terrain, is a characteristic desert area. Sparse vegetation was distributed approximately 500~700 m from the observational station, most of which was *Alhagi sparsifolia*, and *Nitraria tangutorum* Bobr was also present (as shown in Figure 1).

The air temperature and humidity, wind, precipitation, soil temperature (ST, hereinafter) and soil moisture (volumetric water content, VWC hereinafter), land surface radiation, and turbulence were observed. The IOP lasted from June 21st to September 12th. In this paper, the local standard time (LST, hereinafter), which was 7 h ahead of Coordinated Universal Time (UTC), was selected for the calculation and analysis.

The data from August 4th to September 20th were selected for analysis to reflect the effects of rainfall on the soil thermal properties and energy balances in the desert hinterland. During this period, there were two large-scale precipitation events: one occurred on August 18th with 29 mm of precipitation and the other occurred on September 5–7th with 22.6 mm of total precipitation. These events represent rare phenomena in this extremely arid desert area.

2.2. Methods. The hourly precipitation distributions of the two aforementioned synoptic processes are shown in Figure 2, which shows that the first weather event (August 18th) had a short precipitation duration with a high intensity; the maximum rainfall intensity reached 7.8 $mm \cdot h^{-1}$. In contrast, the second weather event had a longer duration, but the maximum intensity was only 2.8 $mm \cdot h^{-1}$. This result indicates that the two precipitation processes were notably different; the first weather event was an extremely intense rainfall episode, the sort of which is typical in the arid region of Northwest China, while the second weather event was characteristic of systematic rainfall.

The sampling frequency of the surface turbulence data was 10 Hz, while the radiometer and soil heat flux plate generated average ST and VWC values, respectively, every 30 min. Basic data quality control measures, such as outlier elimination, time delay correction, virtual temperature correction, and Webb–Pearman–Leuning (WPL) correction,

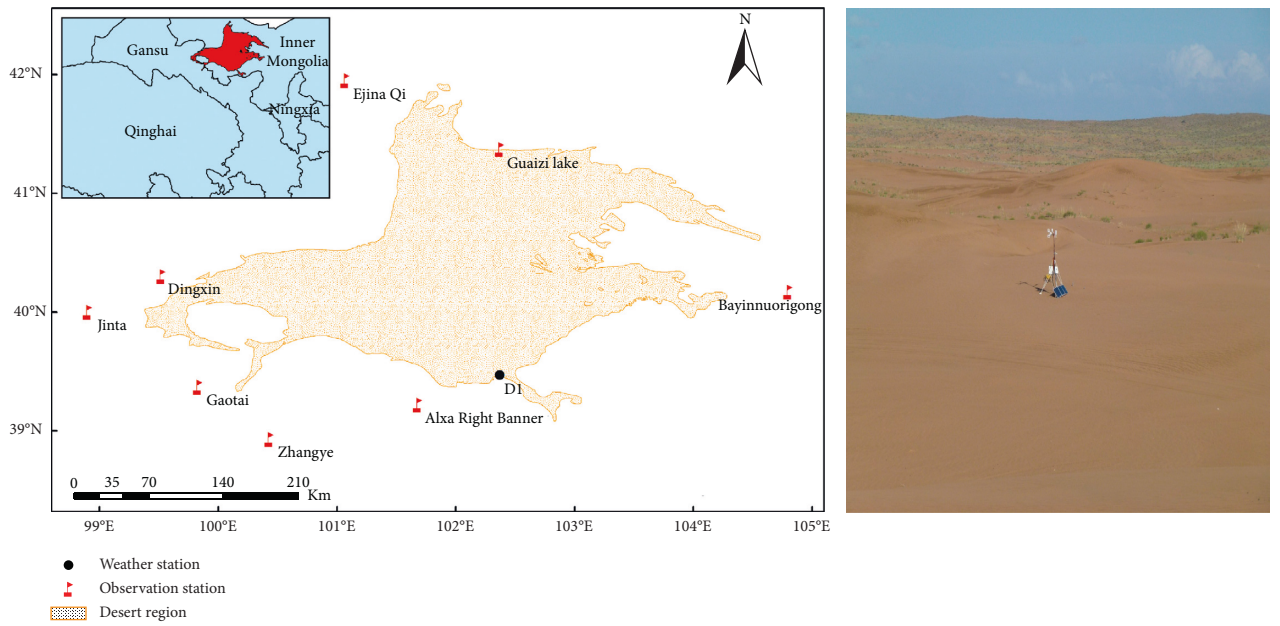

Figure 1: Observation site and surface conditions in the Badain Jaran Desert.

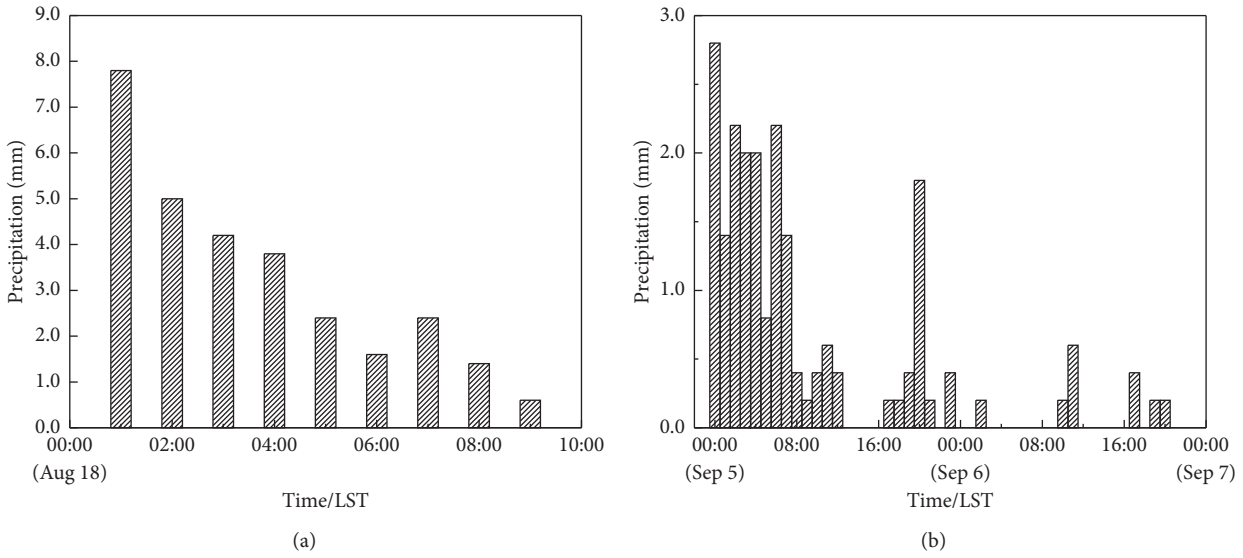

Figure 2: Hourly precipitation distributions of the two weather events: (a) August 18th; (b) September 5–7th.

were applied. To enhance the comparability, only data that had been averaged over 0.5 h intervals and controlled for quality were used for analysis in this paper.

The surface sensible heat flux (H) and latent heat flux (LE) were calculated by the eddy covariance method [34]:

$$H = \rho * C_P * \overline{w'\theta'}, \quad (1)$$

$$\mathrm{LE} = \rho * \lambda * \overline{w'q'}. \quad (2)$$

In formulas (1) and (2), ρ is the air density, C_P is the specific heat at a constant pressure, and λ is the latent heat of evaporation; the latter two are constants. $\overline{w'\theta'}$ and $\overline{w'q'}$ are statistics of the turbulent quantities of the wind temperature and humidity, respectively.

The water-bearing soil volumetric heat capacity C_s, water-free soil volumetric heat capacity C_{sd}, thermal conductivity λ_{si}, and thermal diffusivity K_{si} were calculated according to the following formulas [35]:

$$c_s = \frac{G_1 - G_2}{\Delta z * \left(\partial T_g / \partial t\right)}, \quad (3)$$

$$c_{sd} = \frac{\left(G_1 - G_2\right) - V_w * C_w * \Delta z * \left(\partial T_g / \partial t\right)}{\Delta z * \left(\partial T_g / \partial t\right)}, \quad (4)$$

$$\lambda_{\mathbf{si}} = \frac{G_{\mathrm{i}}}{\partial T_g/\partial z}, \tag{5}$$

$$K_{\mathrm{si}} = \frac{\lambda_{\mathrm{si}}}{C_{\mathrm{s}}}. \tag{6}$$

In formula (3), G_1 and G_2 are the two observed soil heat flux values in the upper (5 cm) and lower (20 cm) layers, respectively, Δz is the thickness between the two observation layers, and $\partial T_g/\partial t$ represents the average ST change rate between the observation depths of the soil heat flux in the two layers. In formula (4), V_{w} is the soil volumetric water content and C_{w} is the specific heat of water, which is $4.2 * 10^3$ J/(kg·°C). In formula (5), G_{i} is the heat flux of the desired soil depth and $\partial T_g/\partial z$ represents the vertical ST gradient.

Since it was difficult to directly measure the surface heat flux, in this paper, the thermal storage in the shallow soil layer was calculated with the thermal diffusion equation and correction (TDEC) method [36]. That is, the surface heat flux was derived by using the measured 5 cm soil layer heat flux and the soil thermal storage of the above 5 cm layer as follows:

$$G_{\mathrm{sfc}} = G_{\mathrm{z}} + S, \tag{7}$$

$$S = \int_{z=0}^{z=z_{\mathrm{ref}}} \rho_{\mathrm{s}} * C_{\mathrm{s}} * \frac{\partial T}{\partial t}\,\mathrm{d}z. \tag{8}$$

In formula (7), G_z and S represent the soil heat flux and thermal storage of the 5 cm layer, respectively. In formula (8), ρ_{s} is the soil density, which is $1.6 * 10^3$ kg·m^{-3} [37]; C_{s} is the soil specific heat; z_{ref} is the reference depth, which is 0.05 m; and $\partial T/\partial t$ represents the temperature change rate between the surface and reference depth.

The following calculation formulas were employed for the surface net radiation R_n, albedo α, and EBR:

$$R_n = R_{\mathrm{SD}} + R_{\mathrm{LD}} - R_{\mathrm{SU}} - R_{\mathrm{LU}}, \tag{9}$$

$$\alpha = \frac{R_{\mathrm{SU}}}{R_{\mathrm{SD}}}, \tag{10}$$

$$\mathrm{EBR} = \frac{\sum (H + \mathrm{LE})}{\sum (R_n - G_{\mathrm{sfc}} - S)}. \tag{11}$$

In formulas (9) and (10), $R_{\mathrm{SD}}, R_{\mathrm{LD}}, R_{\mathrm{SU}}$, and R_{LU} represent the total solar radiation, atmospheric longwave radiation, surface reflective radiation, and surface longwave radiation, respectively. In formula (11), G_{sfc} is the surface heat flux and S is the canopy heat storage capacity, which is equal to zero in the desert area.

3. Results

3.1. Effects of Rainfall on ST and VWC. Figure 3 shows the variations in the ST and before and after rainfall during the two rainfall episodes. Figure 3(a) shows that the VWC values at depths of 5–20 cm were almost equal, and the increase in the VWC value at 40 cm was larger before the first rainfall episode than before the second episode. With the infiltration of rainwater, the VWC increased rapidly, and the VWC increase from shallow to deep layers exhibiting a declining trend, similar to the result of research in the Nebraska Sandhills [27]. Based on the change in the VWC in each layer with time, the VWC was delayed 1.5 h at depths of approximately 5–20 cm and 4 h at depths of 20 and 40 cm. After each rainfall episode, the VWC tended to decrease, and the lapse rate at depths of approximately 5–20 cm was larger than that at a depth of 40 cm and decreased with time. During the second rainfall episode, as the rainfall intensity was relatively small, the growth rate of the VWC was less notable than that during the first rainfall episode. The lag time of the VWC change in each layer was notably prolonged with a 6 h delay at depths between 20 and 40 cm.

Figure 3(b) shows the variations in the soil temperature change rate (TCR, hereafter) before and after the first rainfall episode in various layers. Evidently, the TCR at a depth of 5 cm before rainfall was in the range of −3 to 4°C with a distinct diurnal variation cycle, while the variability in other layers decreased with increasing depth. This phenomenon indicates that the soil was dry, possessed a suitable heat transfer capacity, and was easily influenced by solar radiation in the shallow layer. After rainfall, the TCR notably increased and was negative at depths of approximately 5–10 cm, indicating that the short-term precipitation caused a rapid decrease in the ST while having little effect on the deeper soil layers. During the second rainfall episode, the TCR was similar to that during the first rainfall episode, but its variation was clearly smaller with a longer duration. However, in the deeper layers, the TCR increased to larger values than those during the first rainfall episode; this discrepancy was related to the slow, long-term infiltration of rainwater.

To compare the diurnal variation trends of the TCR between the soil and air, the mean diurnal air TCR and corresponding soil TCR were calculated on rainy and clear days for the entire period, as shown in Figure 4. As rainfall fell, the air TCR changed quickly, while the soil TCR gradually decreased and was lagged by approximately 1 h successively at depths from 5 cm to 20 cm; however, the TCR at a depth of 40 cm changed very little and was lagged by approximately 5 h behind that at a depth of 20 cm (Figure 4(a)). Figure 4(b) shows the same diurnal trends, but the variation in the air TCR was more obvious on clear days. Although there were rapid changes in the air TCR, the overall diurnal trend was consistent with its soil counterpart regardless of the weather.

3.2. Effects of Rainfall on the Surface Albedo. Variations in the soil color, roughness length, VWC, and solar elevation angle can change the surface albedo [38, 39]. As shown in Figure 1, the short-term intense rainfall had a greater impact on the VWC than the long-term systematic rainfall, so the first rainfall episode was selected for analysis.

Figure 5(a) shows that the change in the surface albedo before and after precipitation was not significant, but the surface albedo exhibited a clear reduction during the rainfall

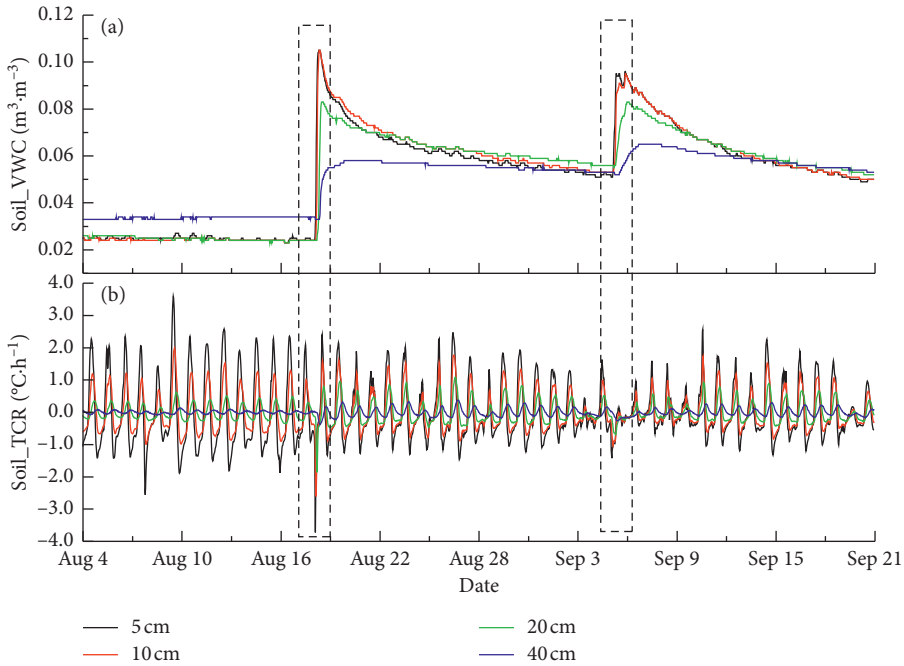

Figure 3: Variations in ST and VWC before and after rainfall: (a) VWC and (b) TCR.

episode. Figure 3(a) also demonstrates that the VWC at a depth of 5 cm decreased the fastest after rainfall, while the surface albedo recovered to a state that was similar to that on the sunny day before the rainfall episode. Additionally, the variation in the surface albedo on the 18th also indicates that the albedo first decreased and then increased due to the increase in the VWC in the surface layer after rainfall, leading to a decrease in the surface albedo. With increasing solar elevation angle and surface temperature, evaporation increased, and the VWC started to decrease, while the surface albedo increased. These trends are similar to those observed in the degraded grasslands of semiarid areas [40].

Figure 5(b) shows the variations in the surface albedo with the solar elevation angle in the desert area. According to the calculations, when the solar elevation angle was greater than 25°, the effect on the surface albedo was very limited, which is somewhat different from the results obtained in the Taklimakan Desert [41]. This difference was caused mainly by the latitude difference between the two locations. Calculations reveal that the solar elevation angle at 7 : 00 LST in the middle of August was approximately 20-21° in the study area. Therefore, the solar elevation angle had little effect on the surface albedo before and after rainfall; instead, the albedo was related to the smooth underlying surface and less pronounced topographic undulation in the desert.

3.3. Effects of Rainfall on the Soil Thermal Parameters. Figure 3 shows that the ST and VWC varied greatly before and after the rainfall event on August 18th. Thus, periods of a week before and after the rainfall episode (August 12–24th) were selected for analysis, where August 12–17th and August 19–24th were chosen as the periods before and after the rainfall episode, respectively.

Figure 6(a) shows that the soil thermal capacity before the rainfall event was 1.09×10^6 J·m^{-3}·K^{-1}, which is close to the measured value of 1.12×10^6 J·m^{-3}·K^{-1} [42] in Dunhuang and slightly lower than the result of 1.56×10^6 J·m^{-3}·K^{-1} in the Taklimakan Desert [41]. After rainfall (Figure 6(b)), the soil thermal capacity increased to 1.54×10^6 J·m^{-3}·K^{-1} due to the increase in the VWC and a lower air content between sand particles, which resulted in an increase in the soil thermal capacity. As shown in Figures 6(c) and 6(d), the water-free soil thermal capacity increased notably before and after rainfall, respectively.

To better understand the influence of the VWC on the soil heat capacity, the variations in the soil thermal capacity with the VWC in the water-bearing and water-free soils after rainfall were analyzed, as shown in Figure 7. The two kinds of soil exhibited similar trends: the soil thermal capacity slowly increased with increasing soil VWC.

Figure 8 shows that the soil thermal conductivity at a depth of 5 cm (in the shallow layer) before rainfall was only 0.23 W·m^{-1}·K^{-1}, which is close to the measured value in the hinterland of the Taklimakan Desert; after rainfall, the value more than doubled to 0.66 W·m^{-1}·K^{-1}. The soil thermal conductivity at a depth of 20 cm after rainfall was approximately 5 times that before rainfall. From a vertical depth perspective, the soil thermal conductivity in the middle layer was only slightly higher than that in the shallow layer before rainfall but was twice that in the shallow layer after rainfall. The main reason for this phenomenon is that the solar radiation of the middle layer before rainfall was smaller due to a higher VWC. The aforementioned conditions resulted in a small thermal conductivity difference between the middle and shallow layers due to the dry yellow sand surface covering the desert (Figure 3(a)). After rainfall, similar to the principle governing the increase in the soil thermal capacity, the VWC

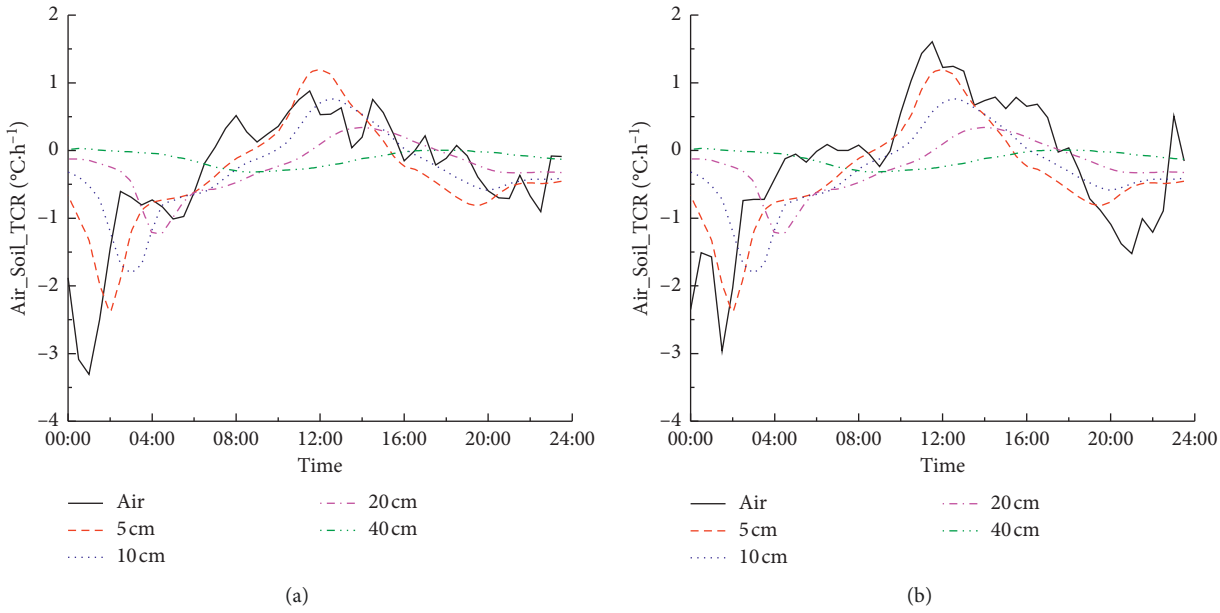

Figure 4: Diurnal TCR variation in the air and in each layer: (a) rainy days and (b) clear days.

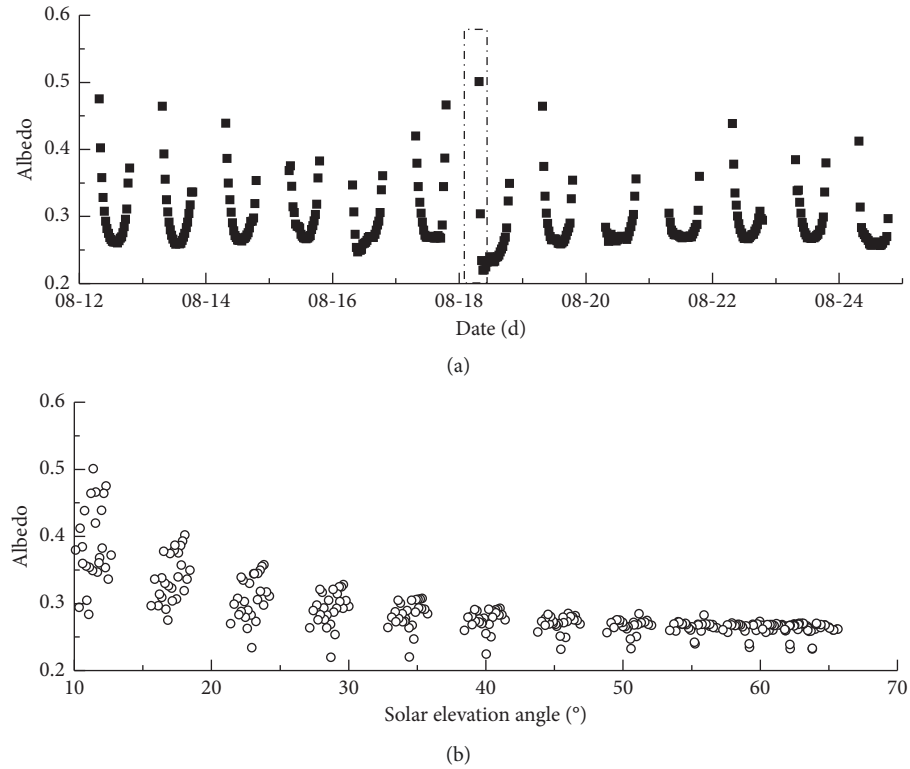

Figure 5: (a) Variations in the surface albedo before and after rainfall (the dashed-dotted rectangle represents the short-term rainfall period); (b) variations in the surface albedo at different solar elevation angles.

values in the middle and shallow layers exhibited a declining trend due to evaporation. A soil moisture inversion phenomenon appeared before August 22nd but gradually disappeared afterward. The VWC at a depth of 20 cm was greater than those at the other depths. Therefore, there was a large variation in the soil thermal conductivity in the middle layer after rainfall. This finding ultimately indicates that rainfall had a large effect on the soil above a depth of 20 cm, while the effect on the soil below 20 cm was relatively small.

The soil thermal diffusivity represents the instantaneous change in ST with the given boundary conditions. According to the formulas in this paper, the soil thermal diffusivity

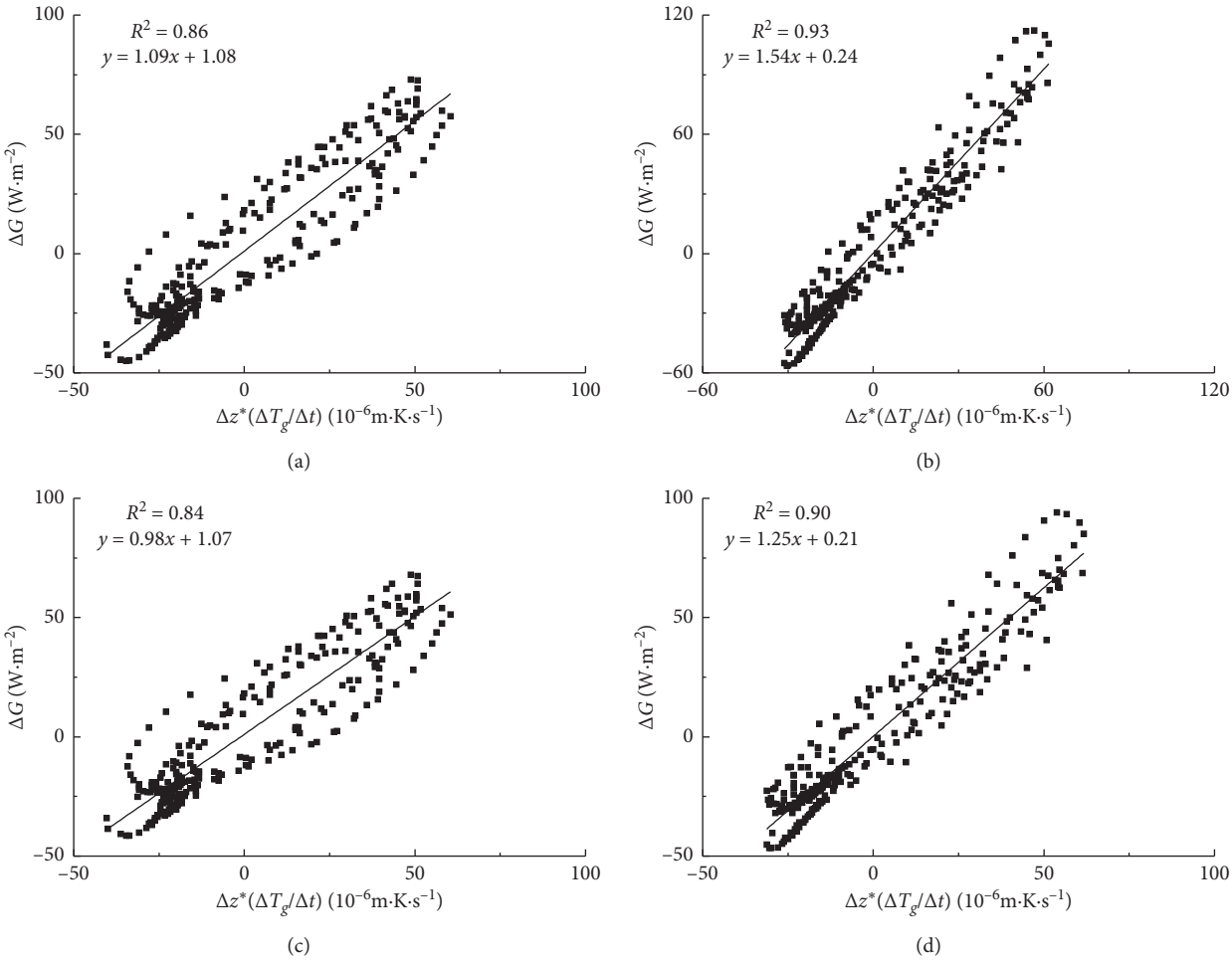

Figure 6: Variations in the soil thermal capacity before and after rainfall: (a) water-bearing soil before rainfall; (b) water-bearing soil after rainfall; (c) water-free soil before rainfall; (d) water-free soil after rainfall.

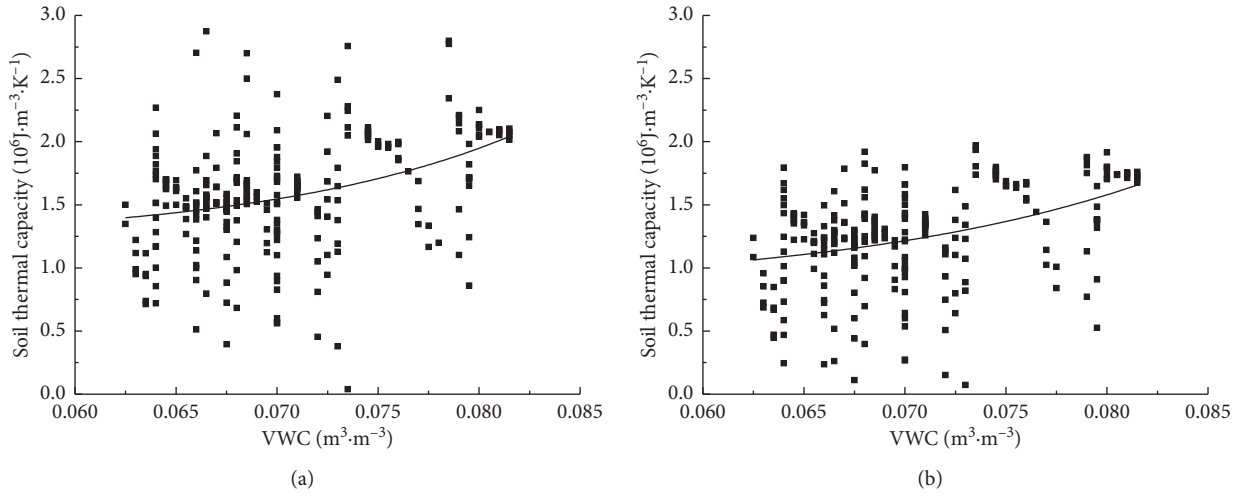

Figure 7: Variations in the soil thermal capacity with the VWC: (a) water-bearing soil and (b) water-free soil.

values before and after rainfall were calculated as 2.1×10^{-7} m^2·s^{-1} and 4.3×10^{-7} m^2·s^{-1}, respectively, at a depth of 5 cm and 2.8×10^{-7} m^2·s^{-1} and 9.4×10^{-7} m^2·s^{-1}, respectively, at a depth of 20 cm.

Based on the above analysis, the rainfall episodes had considerable effects on the soil thermal parameters in the desert area, indicating that the soil volumetric heat capacity, thermal conductivity, and thermal diffusivity after rainfall all

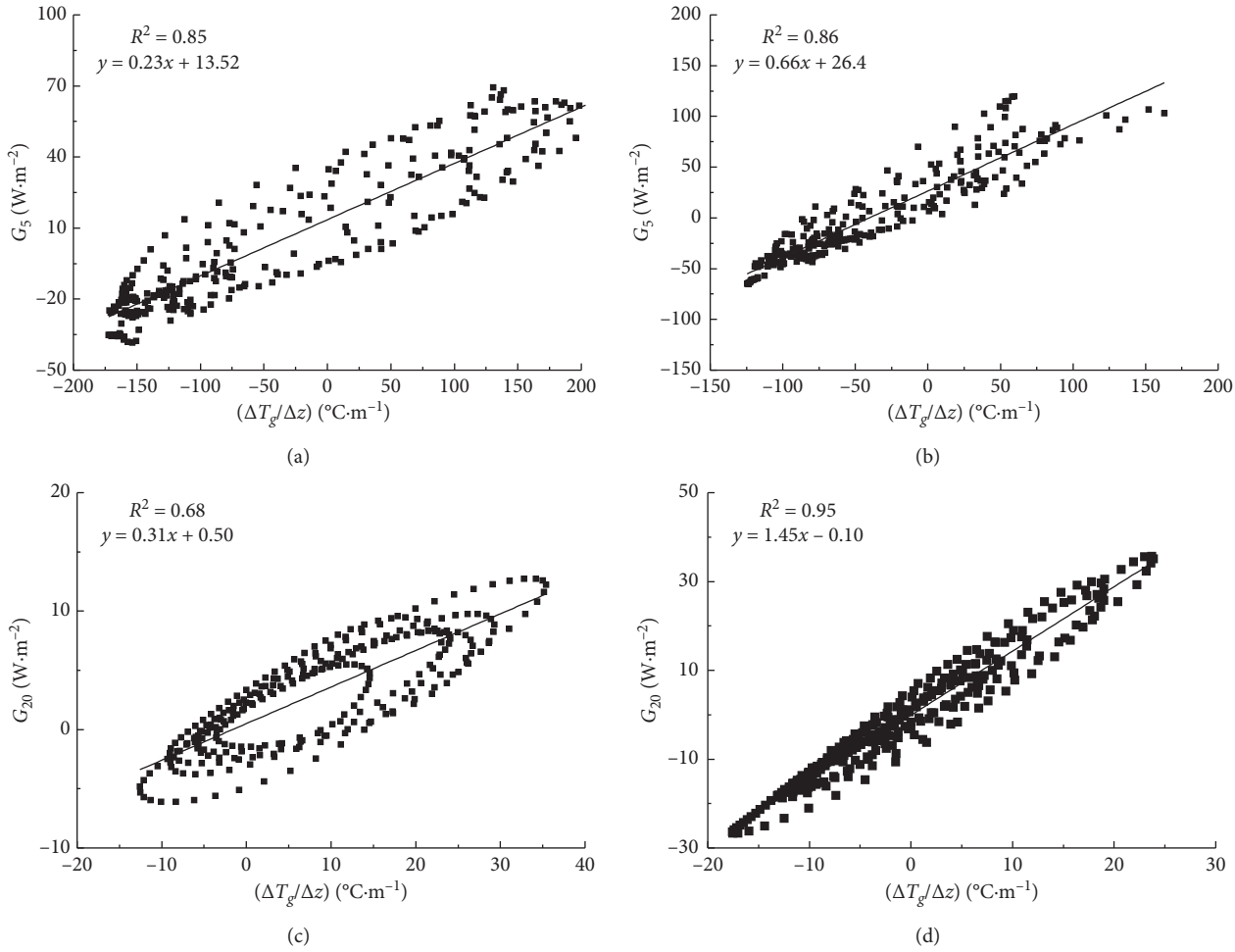

Figure 8: Variations in the soil thermal conductivity before and after rainfall: (a) 5 cm depth before rainfall; (b) 5 cm depth after rainfall; (c) 20 cm depth before rainfall; (d) 20 cm depth after rainfall.

significantly increased in comparison with those before rainfall. Moreover, the growth rates of the soil thermal conductivity and thermal diffusivity in the middle layer were notably higher than those in the shallow layer. Moreover, with respect to the Dunhuang Gobi and hinterland of the Taklimakan Desert, the soil thermal conductivity and thermal diffusivity in the Badain Jaran Desert were slightly higher.

3.4. Effects of Rainfall on the Surface Energy Balance. The soil heat flux is an integral part of the surface energy balance and plays an important role in the distribution of surface energy. Correctly estimating the soil heat flux can significantly improve the surface energy imbalance, particularly in bare or sparsely vegetated ground [43].

Figure 9(a) shows the variation in the global solar radiation before and after the first rainfall episode. The weather was clear with dry air and a suitable atmospheric transparency before rainfall; accordingly, the diurnal variation curve of the global solar radiation was relatively smooth, and the daily extremes were all close to 1000 W·m^{-2}. The latter observation indicates that the solar radiation in the desert was intense at this time. Additionally, because rainfall usually occurred in the nighttime, its effect on solar radiation was less pronounced. After the rainfall event, the weather gradually cleared up, but clouds easily formed due to the large amount of water vapor evaporation and atmospheric vertical motion, resulting in reduced solar radiation. Therefore, the daily global solar radiation peak decreased slightly after rainfall with respect to that before rainfall.

Figure 9(b) shows the variations in the soil heat flux at depths of 5 and 20 cm before and after rainfall. Clearly, the soil heat flux exhibited distinct diurnal variations resembling quasisinusoids in all layers. Moreover, these fluctuations gradually decreased with increasing depth. With respect to that in the shallow layer, the variation in the soil heat flux in the middle layer before and after rainfall lagged by approximately 4 h. Furthermore, the solar radiation was weaker during the rainfall episode than before or after. Compared with the atmosphere, the land surface became a cold source. Soil heat was released from deeper layers to the surface layer, and thus, the surface layer exhibited a large negative value (shown in the dotted box in Figure 9(b)). Even under the circumstances involving a small variation in the total radiation, the fluctuation in the soil heat flux in all

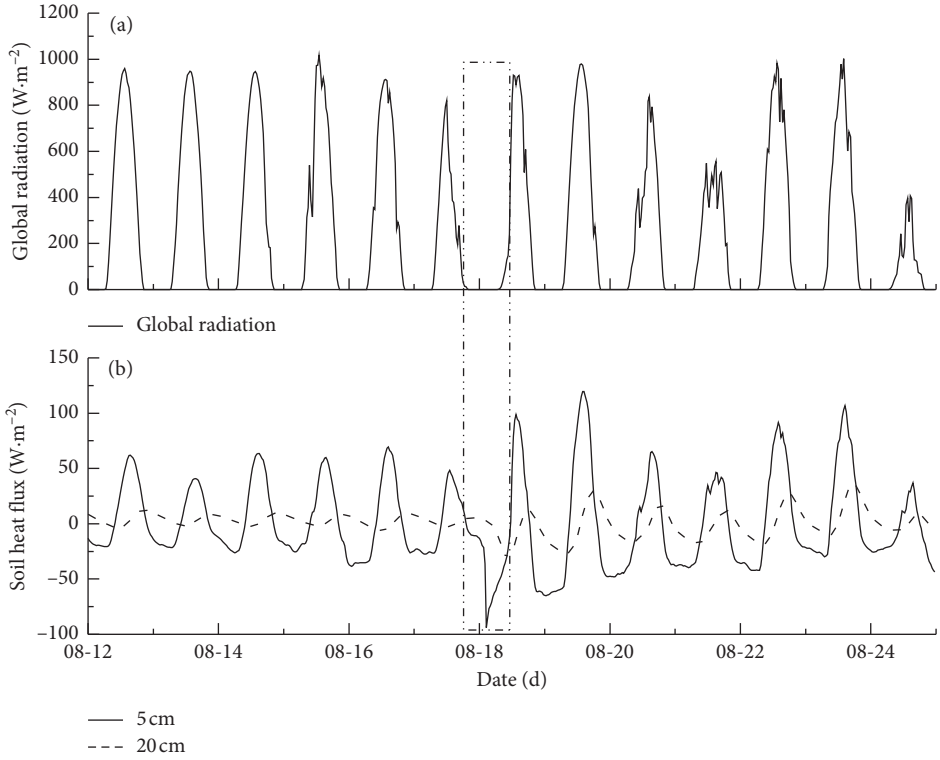

Figure 9: Variations in the (a) global solar radiation and (b) soil heat flux before and after rainfall.

layers after rainfall increased in comparison with that before rainfall. The cause of this enhanced fluctuation is attributed to the decrease in the surface albedo after rainfall, the relative increase in the amount of heat entering the soil, and the significant increases in the soil thermal parameters, including the soil volumetric heat capacity, compared with those before rainfall. As a result, the soil absorbed a larger amount of heat in the daytime and released a larger amount of heat in the nighttime.

Figures 10(a) and 10(c) depict the variations in the EBR without S (thermal storage in the 5 cm layer) before and after rainfall, respectively, during the daytime (08 : 00–17 : 00 LST). These figures demonstrate that the EBR, which was 0.62 before rainfall, decreased to 0.50 after the rainfall episode. Two reasons can explain this phenomenon. On the one hand, in this desert area, the vegetation was sparse, the latent heat on a sunny day was small, and the surface energy was transported primarily by sensible heat [44]. Therefore, the surface sensible heat flux reached a maximum value of 400 W·m^{-2}, whereas the daily latent heat flux extreme reached only approximately 45 W·m^{-2}. Although the VWC increased after rainfall, resulting in a notable increase in the latent heat flux with a maximum exceeding 150 W·m^{-2}, the latent heat flux decreased rapidly with the gradual decline in the VWC. However, the sensible heat flux decreased after rainfall due to variations in the soil thermal properties and weather effects. As a result, the turbulent energy (calculated as Hs + LE) was notably reduced. On the other hand, although the soil heat flux at a depth of 5 cm after rainfall slightly increased (Figure 9(b)), the net radiation slightly decreased due to the reduction in the global solar radiation. As a result, the effective energy (calculated as $R_n - G$) slightly decreased.

The EBR values with S before and after rainfall are shown in Figures 10(b) and 10(d), respectively. Clearly, the EBR with S increased approximately 5-6% before and after rainfall, indicating that S in the surface layer had an important contribution to the surface energy balance in this desert area. From these figures, the EBR with S after rainfall was still lower than that before rainfall. The main reason for this phenomenon is that the soil thermal capacity and density both increased with increasing VWC in the shallow layer after rainfall. As a result, S became larger, intensifying the surface energy imbalance.

Figure 11 shows the overall variation trends in the EBR in the daytime before and after the two rainfall episodes. Clearly, the EBR increased slowly because of the suitable weather conditions before rainfall and reached a maximum value that was affected by the surface properties and weather conditions. After rainfall, the EBR gradually decreased again. Additionally, the EBR after rainfall was slightly lower than that before rainfall. Figure 10(b) shows that the average EBR with S was 0.61, which represented an increase of 6% in comparison with that without S.

The above analysis illustrates that the EBR remained low during both the short-term and the systematic rainfall episodes as a result of the profound energy imbalance in the desert area. Many reasons were responsible for this phenomenon, which requires further study.

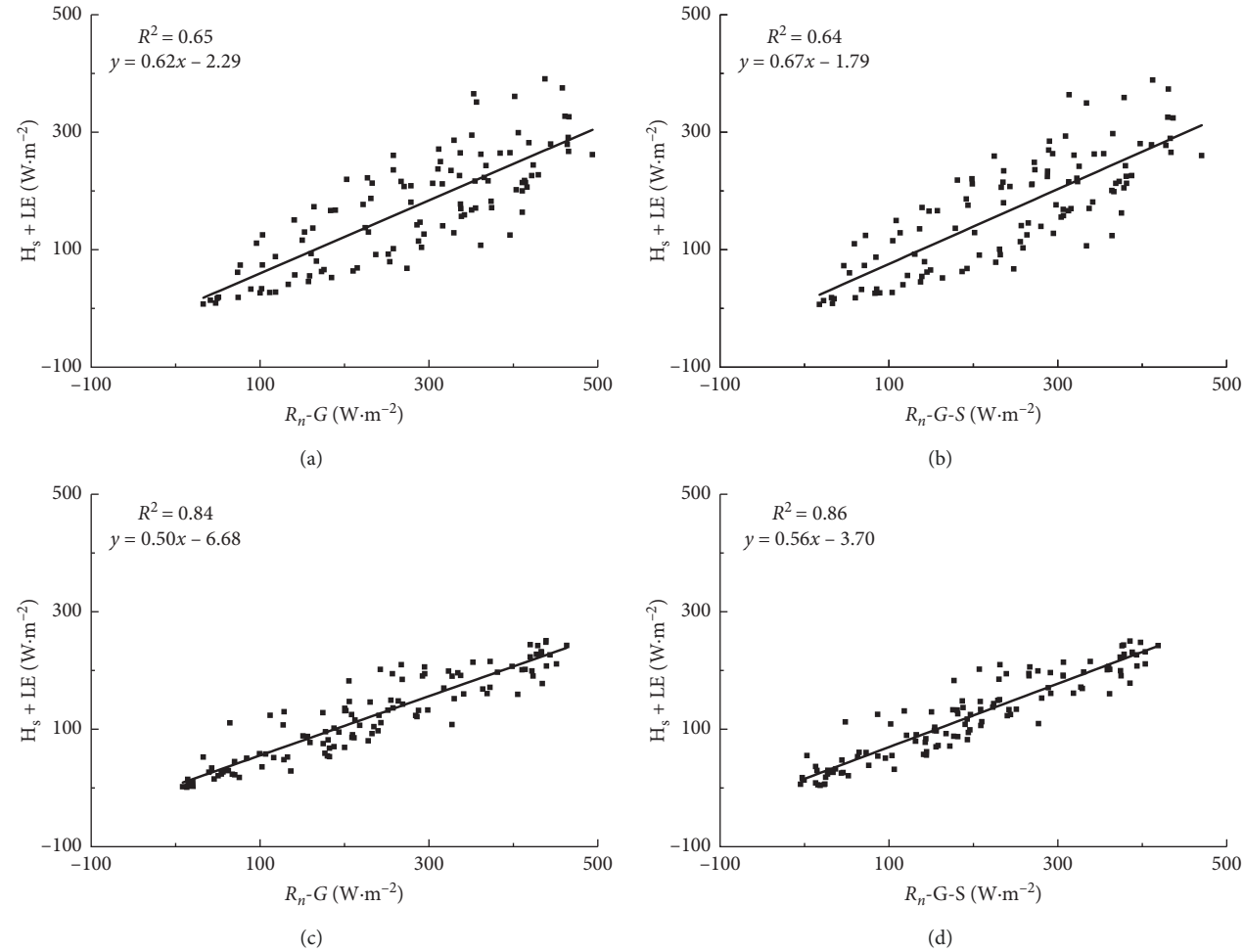

Figure 10: Variations in the EBR before and after rainfall: (a) without *S* before rainfall; (b) with *S* before rainfall; (c) without *S* after rainfall; (d) with *S* after rainfall.

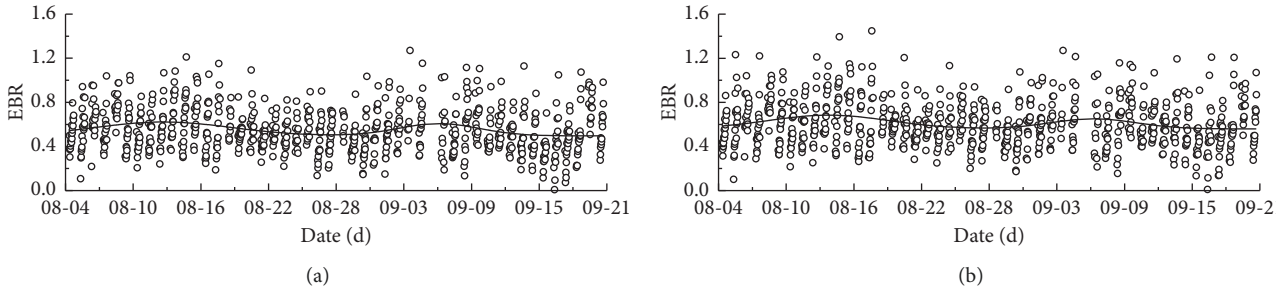

Figure 11: EBR variation trends during the entire observation period: (a) without *S* and (b) with *S*.

4. Discussion

The annual precipitation and number of annual rainy days at the tops of the sand mountains in the Badain Jaran Desert were slightly higher than those in the fields surrounding the hills [45]; thus, the responses of the soil properties to rainfall in different desert terrains also differed. Therefore, the results in this paper were adapted to only relatively flat desert areas. Additionally, rainfall episodes with different intensities had different effects on the VWC and thermal parameters, as shown by field testing in the Loess Plateau [46], which is in agreement with the results in this paper. However, there was no notable wet layer in the studied desert area.

It is generally acknowledged that the soil color and roughness length do not experience significant dynamic changes; thus, the surface albedo depends on the solar elevation angle and VWC. The variation in albedo during the rainfall episodes indicated that the short-term rainfall episode in the desert area had little effect on the surface albedo

because the clear day solar radiation was intense and the evaporation potential was very large. The latter phenomenon resulted in the VWC rapidly evaporating out of the layer closest to the surface in this area.

A possible reason for the rapid increase in the VWC after rainfall and the decreased growth rate from the shallow layer to the deep layers mentioned earlier was the infiltration of rainwater after rainfall. Although the VWC in the shallow layer gradually decreased with an increase in solar radiation after the sky cleared up, the sandy soil surface easily formed a hardened layer, leading to a reduction in the shallow soil porosity. This porosity reduction caused the liquid water in the subsoil to evaporate slowly. The soil thermal capacity serves as an indicator of the degree of change in the ST, and the thermal capacity varies greatly with different soil components; consequently, there are notable differences in the thermal capacities of soils with different compositions. The greater the thermal capacity, the slower the ST change; this phenomenon is commonly known as cold soil and occurs in sticky soil, while the opposite phenomenon is called hot soil and occurs in light sandy soil. The soil heat flux calculations at observation depths of 5 and 20 cm were based mainly on shallow soil. Similarly, the soil heat capacity was considered to be equal at depths of 0–20 cm, while the value of S was calculated. It is common to replace the thermal capacity of the layer above 5 cm with those of the layers at depths of 5–20 cm. In the desert area, the soil in the shallow layer was dry, while the change in the subsoil moisture was more profound. Therefore, the proposed method needs to be further improved and researched in the studied desert area.

The soil thermal conductivity represents the soil heat transfer performance and constitutes the basic physical parameter for studying coupled hydrothermal motions on land surfaces. The soil thermal conductivity depended mainly on the VWC, tightness, and porosity. Generally, light soil was better than sticky soil in terms of the thermal conductivity. With an increase in the VWC, the thermal conductivity was enhanced; as a result, the soil thermal conductivity clearly increased after rainfall in this paper. The soil particles in the desert were small, resulting in intense water absorption and a poor water permeability of the soil. Therefore, during both short-term heavy rainfall and systematic persistent precipitation, the responses of the ST and VWC in the shallow layer were more rapid than those in the deeper layers. However, the impact duration time was short, which led to results that are consistent with the results reported by other domestic scholars. However, due to differing soil properties, the effects of rainfall on the soil at different depths, terrains, ST and VWC values, and soil thermal parameters were not the same. In this experiment, a sandy soil density was used before and after rainfall because the exact soil density had not been measured, which may have had a certain effect on the EBR calculations. In addition, the vegetation type and coverage also affected the aforementioned parameters. Therefore, there are still several remaining issues worthy of exploration.

5. Conclusions

In this paper, the effects of rainfall episodes on the surface albedo, soil thermal parameters and EBR in the Badain Jaran Desert were analyzed; the results of this investigation are the key to improving the parameterization of the surface radiation budget and energy balance for numerical models in semiarid areas. In summary, several characteristic observations were made as follows:

(1) Short-term rainfall had a large influence on the ST and VWC compared with systematic precipitation. The VWC increased rapidly after rainfall with a decreased growth rate from the shallow layer to the deep layers. The TCR in the shallow layer notably decreased after rainfall and increased in the deep layers. The surface albedo during the short-term rainfall episode was significantly reduced and exhibited little change before and after rainfall. The solar elevation angle had little effect on the surface albedo before and after rainfall; instead, the surface albedo was related to the smooth underlying desert surface.

(2) The soil thermal conductivity clearly increased after rainfall. The water-free soil thermal conductivity followed the same trend that was related to the decreased porosity caused by the hardened layer, which easily formed in the sandy soil surface after rainfall, and by the slower evaporation of the liquid water in the subsoil relative to the water at the surface. With an increasing VWC, the soil thermal capacity, thermal diffusivity, and thermal conductivity slowly increased after rainfall. From a vertical depth perspective, the soil thermal conductivity growth rate in the middle layer was larger than that in the shallow layer before and after rainfall; similar trends were observed for the thermal diffusivity.

(3) The diurnal variation curve of the global solar radiation was relatively smooth before rainfall, and the daily extremes reached nearly 1000 $W \cdot m^{-2}$. The soil heat flux in each layer exhibited distinct diurnal variations resembling quasisinusoids. The fluctuation in the soil heat flux gradually decreased with increasing depth and increased in each layer after rainfall. The change in the soil heat flux in the middle layer lagged by approximately 4 h compared to that in the shallow layer.

(4) The EBR without S was 0.62 before rainfall but decreased to 0.50 after rainfall. Regardless of the occurrence of rainfall, the EBR with S increased by approximately 5-6%; however, the EBR was still lower after rainfall than before. Throughout the entire observation period, the EBR in the daytime reached a maximum at approximately 1-2 days before or after rainfall and gradually declined at other times.

Data Availability

The observation data used to support the findings of this study were supplied by the National Natural Science Foundation of China (41505008 and 41675020) under license and so cannot be made freely available. Requests for access to these data should be made to Zhaoguo Li (zgli@lzb.ac.cn).

Conflicts of Interest

The authors declare that they have no conflicts of interest.

Acknowledgments

This research was funded by the National Natural Science Foundation of China (41875023, 41505008, 41675020, and 41575008) and the China Special Fund for Meteorological Research in the Public Interest (GYHY201506001-04 and GYHY201306066).

References

[1] J. W. Raich and A. Tufekciogul, "Vegetation and soil respiration: correlations and controls," *Biogeochemistry*, vol. 48, no. 1, pp. 71–90, 2000.

[2] D. Gaumont-Guay, T. A. Black, T. J. Griffis et al., "Interpreting the dependence of soil respiration on soil temperature and water content in a boreal aspen stand," *Agricultural and Forest Meteorology*, vol. 140, no. 1–4, pp. 220–235, 2006.

[3] A. Haines, "Climate change 2001: the scientific basis. Contribution of working group 1 to the third assessment report of the intergovernmental panel on climate change," *International Journal of Epidemiology*, vol. 32, no. 2, p. 321, 2003.

[4] V. Sridhar, W. T. A. Jaksa, B. Fang et al., "Evaluating bias-corrected AMSR-E soil moisture using in situ observations and model estimates," *Vadose Zone Journal*, vol. 12, no. 3, pp. 1712–1717, 2013.

[5] W. T. Jaksa and V. Sridhar, "Effect of irrigation in simulating long-term evapotranspiration climatology in a human-dominated river basin system," *Agricultural and Forest Meteorology*, vol. 200, pp. 109–118, 2015.

[6] Y. Gao, G. Cheng, W. Liu et al., "Modification of the soil characteristic parameters in Heihe River basin and effects on simulated atmospheric elements," *Plateau Meteorology*, vol. 5, no. 8, 2007, in Chinese.

[7] Y. Gao, W. Liu, G. Cheng, H. Peng, H. Li, and Y. Ran, "Setup and validation of the soil texture type distribution data in the Heihe River basin," *Plateau Meteorology*, vol. 26, no. 5, pp. 967–974, 2007, in Chinese.

[8] M. F. Wilson, A. Henderson-Sellers, R. E. Dickinson, and P. J. Kennedy, "Sensitivity of the biosphere-atmosphere transfer scheme (BATS) to the inclusion of variable soil characteristics," *Journal of Climate and Applied Meteorology*, vol. 26, no. 3, pp. 341–362, 1987.

[9] Q. Zhang, "Simple review of land surface process model," *Scientia Meteorologica Sinica*, vol. 18, no. 3, pp. 295–304, 1998, in Chinese.

[10] L. Gan, X. Peng, S. Peth, and R. Horn, "Effects of grazing intensity on soil thermal properties and heat flux under Leymus chinensis and Stipa grandis vegetation in Inner Mongolia, China," *Soil and Tillage Research*, vol. 118, pp. 147–158, 2012.

[11] S. Park, J. J. Feddema, and S. L. Egbert, "Impacts of hydrologic soil properties on drought detection with MODIS thermal data," *Remote Sensing of Environment*, vol. 89, no. 1, pp. 53–62, 2004.

[12] F. Wang, J. L. Dufresne, C. Frédérique, and D. Agnès, "The effects of soil vertical discretization, soil thermal properties, and soil heat convection by liquid water transfer on the water and energy cycles in a coupled land-atmosphere model," *Geophysical Research*, vol. 17, 2015.

[13] B. P. Guillod, B. Orlowsky, D. Miralles et al., "Soil moisture-precipitation coupling: observations question an impact on precipitation occurrence in North America," *Proceedings of European Geosciences Union General Assembly*, vol. 15, 2013.

[14] B. M. Lofgren, "Sensitivity of land-ocean circulations, precipitation, and soil moisture to perturbed land surface albedo," *Journal of Climate*, vol. 8, pp. 2521–2542, 2009.

[15] J. Otterman, "Enhancement of surface-atmosphere fluxes by desert-fringe vegetation through reduction of surface albedo and of soil heat flux," *Theoretical & Applied Climatology*, vol. 40, no. 1-2, pp. 67–79, 1989.

[16] V. Sridhar and D. A. Wedin, "Hydrological behaviour of grasslands of the Sandhills of Nebraska: water and energy-balance assessment from measurements, treatments, and modelling," *Ecohydrology*, vol. 2, no. 2, pp. 195–212, 2009.

[17] V. Sridhar, K. G. Hubbard, and D. A. Wedin, "Assessment of soil moisture dynamics of the Nebraska Sandhills using Long-Term measurements and a hydrology model," *Journal of Irrigation and Drainage Engineering*, vol. 132, no. 5, pp. 463–473, 2006.

[18] Q. Zhang, W. Guoan, S. Wang, and X. Hou, "Vertical change of the soil structure parameters and the soil thermodynamic para meters in the Gobi deserts in arid areas," *Arid Zone Research*, vol. 20, no. 1, pp. 44–52, 2003, in Chinese.

[19] Q. Zhang and Y. Hu, "The flux-profile relationships under the condition of heat advection over moist surface," *Scientia Atmospherica Sinica*, vol. 19, no. 1, 1995, in Chinese.

[20] Y. Hu and Y. Gao, "Some new understandings of processes at the land surface in arid area from the HEIFE," *Acta Meteorologica Sinica*, vol. 52, no. 3, pp. 285–296, 1994, in Chinese.

[21] Y. Hu, "Preliminary analysis about characteristics of microclimate and heat energy budget in HEXI GOBI," *Plateau Meteorology*, vol. 9, no. 2, pp. 113–119, 1990, in Chinese.

[22] Q. Zhang and X. Cao, "The influence of synoptic conditions on the averaged surface heat and radiation budget energy over desert or Gobi," *Chinese Journal of Atmospheric Sciences*, vol. 27, no. 2, pp. 245–254, 2003, in Chinese.

[23] Z. Yang, X. Li, Y. SUN, L. Liu, X. Zhang, and Y. Ma, "Characteristics of rainfall interception and stemflow for Salix psammophila in Maowusu sandland, Northwest China," *Advances in Water Science*, vol. 19, no. 5, pp. 693–698, 2008, in Chinese.

[24] J. You, K. G. Hubbard, R. Mahmood, V. Sridhar, and D. Todey, "Quality control of soil water data in applied climate information system-case study in Nebraska," *Journal of Hydrologic Engineering*, vol. 15, no. 3, pp. 200–209, 2010.

[25] K. G. Hubbard, J. You, V. Sridhar, E. Hunt, S. Korner, and G. Roebke, "Near-surface soil-water monitoring for water resources in management on a wide-area basis in the Great Plains," *Great Plains Research*, vol. 19, no. 1, pp. 45–54, 2009.

[26] V. Sridhar, "Tracking the influence of irrigation on land surface fluxes and boundary layer climatology," *Journal of Contemporary Water Research & Education*, vol. 152, no. 1, pp. 79–93, 2013.

[27] V. Sridhar and K. G. Hubbard, "Estimation of the water balance using observed soil water in the Nebraska Sandhills," *Journal of Hydrologic Engineering*, vol. 15, no. 1, pp. 70–78, 2010.

[28] Q. He and M. Xiang, "Analyzed on a heavy precipitation in the hinterland of Taklimakan desert," *Arid Zone Research*, vol. 15, no. 1, pp. 15–20, 1998, in Chinese.

[29] Z. Yang, W. Chen, G. Chen, and Z. Dong, "Characteristics of the weather in the hinterland of the Taklimakan desert," *Journal of Desert Research*, vol. 15, no. 3, pp. 293–298, 1995, in Chinese.

[30] D. Sun and J. Yang, "Precipitation characteristics at the hinterland of Gurbantunggut desert and the surrounding areas," *Arid Land Geography*, vol. 33, no. 5, pp. 769–774, 2010, in Chinese.

[31] K. Zhang, Z. Yao, Z. An, and S. Xie, "Wind-blown sand environment precipitation over the Badain Jaran Desert and its adjacent regions," *Journal of Desert Research*, vol. 32, no. 5, pp. 442–466, 2012, in Chinese.

[32] J. Zhu, N. A. Wang, H. B. Chen, C. Y. Dong, and H. A. Zhang, "Study on the boundary and the area of Badain Jaran Desert based on remote sensing imagery," *Progress in Geography*, vol. 29, no. 9, pp. 1087–1094, 2010, in Chinese.

[33] N. Ma and X. Yang, "Environmental isotopes and water chemistry in the Badain Jaran Desert and in its southeastern adjacent areas, inner Mongolia and their hydrological implications," *Quaternary Sciences*, vol. 28, no. 4, pp. 702–711, 2008, in Chinese.

[34] D. A. Haugen, J. C. Kaimal, and E. F. Bradley, "An experimental study of Reynolds stress and heat flux in the atmospheric surface layer," *Quarterly Journal of the Royal Meteorological Society*, vol. 97, no. 412, pp. 168–180, 2010.

[35] Z. Qiang and H. Ronghui, "Parameters of land-surface processes for Gobi in north-west China," *Boundary-Layer Meteorology*, vol. 110, no. 3, pp. 471–478, 2004.

[36] K. Yang and J. Wang, "A temperature prediction correction method for calculating surface soil heat flux based on soil temperature and humidity data," *Science In China Press*, vol. 38, no. 2, pp. 243–250, 2008, in Chinese.

[37] J. P. Peixóto and A. H. Oort, "Physics of climate," *Reviews of Modern Physics*, vol. 56, no. 365, 1984.

[38] Q. Zhang, R. Huang, S. Wang, W. Guoan, X. Cao, and X. Hou, "NWC-ALIEX and its research advances," *Advances In Earth Science*, vol. 20, no. 4, pp. 427–441, 2005.

[39] H. Liu, B. Wang, and C. Fu, "Relationships between surface albedo, soil thermal parameters and soil moisture in the semi-arid area of Tongyu, northeastern China," *Advances in Atmospheric Sciences*, vol. 25, no. 5, pp. 757–764, 2008.

[40] Z. Liu, G. Tu, and W. Dong, "The variation characteristics of albedo in different surface of semi-arid region," *Science in China Press*, vol. 53, no. 10, pp. 1220–1227, 2008, in Chinese.

[41] Y. Liu, Q. He, H. Zhang, and M. Ali, "Studies of land-atmosphere interaction parameters in Taklimakan Desert hinterland," *Plateau Meteorology*, vol. 30, no. 5, pp. 1294–1299, 2011, in Chinese.

[42] Q. Zhang, X. Cao, G. Wei, and R. Huang, "Observation and study of land surface parameters over Gobi in typical arid region," *Advances in Atmospheric Sciences*, vol. 19, no. 1, pp. 121–135, 2002.

[43] B. G. Heusinkveld, A. F. G. Jacobs, A. A. M. Holtslag, and S. M. Berkowicz, "Surface energy balance closure in an arid region: role of soil heat flux," *Agricultural and Forest Meteorology*, vol. 122, no. 1-2, pp. 21–37, 2004.

[44] J. Li, Y. Ao, and Z. Li, "Comparative analysis of radiation and energy budget over Badain Jaran Desert on clear and cloudy days in summer," *Progress in Geography*, vol. 31, no. 11, pp. 1443–1451, 2012, in Chinese.

[45] N. Wang, N. Ma, H. B. Chen, X. L. Chen, C. Y. Dong, and Z. Y. Zhang, "A preliminary study of precipitation characteristics in the hinterland of Badain Jaran Desert," *Advances in Water Science*, vol. 24, no. 2, pp. 2153–2160, 2013, in Chinese.

[46] P. Yue, Q. Zhang, J. Yang et al., "Surface heat flux and energy budget for semi-arid grassland on the Loess Plateau," *Acta Ecologica Sinica*, vol. 31, no. 22, pp. 6866–6876, 2011, in Chinese.